DE GRUYTER

Curved and Layer. Struct. 2021; 8:109–118

Research Article

Erica Lenticchia, Amedeo Manuello Bertetto*, and Rosario Ceravolo

AE propagation velocity calculation for stiffness estimation in Pier Luigi Nervi's concrete structures**

Abstract: In the present paper, the acoustic emission (AE) device is used with an innovative approach, based on the calculation of P-wave propagation velocity (v_p), to detect the stiffness characteristics and the diffused damage of in-service old concrete structures. The paper presents the result of a recent testing campaign carried out on the slant pillars composing the vertical bearing structures designed by Pier Luigi Nervi in one of his most iconic buildings: the Hall B of Torino Esposizioni. In order to investigate the properties of these inclined pillars, localizations of artificial sources (hammer impacts), by the triangulation procedure, were performed on three different inclined elements characterized by stiffness discrepancies due to different causes: the casting procedures, executed in different stages, and the enlargement of the hall happened a few years later the beginning of the construction. In the present work, the relationship between the velocity of AE signals and the elastic characteristics (principally elastic modulus, E) is evaluated in order to discriminate the stiffness level of the slanted pillars. The procedure presented made it possible to develop an innovative investigation method able to estimate, by means of AE, the state of conservation and the elastic properties and the damage level of the monitored concrete and reinforced concrete structures.

Keywords: 20th century architectural heritage, old reinforced concrete, AE wave propagation velocity, stiffness estimation, damage in concrete, localization, NDT

*Corresponding Author: Amedeo Manuello Bertetto: Department of Structural, Geotechnical and Building Engineering, Politecnico di Torino – Torino, Italy; Email: amedeo.manuellobertetto@polito.it
Erica Lenticchia, Rosario Ceravolo: Department of Structural, Geotechnical and Building Engineering, Politecnico di Torino – Torino, Italy; Responsible, Risk, Resilience Interdepartmental Centre (R3C), Politecnico di Torino, Corso Duca degli Abruzzi 24, 10129 Torino, Italy

1 Introduction

The present work is part of the topical line of analysis and structural diagnosis aimed at the conservation of the architectural heritage of the 20th century; a heritage of great importance but characterized by several problems. In fact, the buildings of the 20th century present specific issues, connected to the materials and techniques used for the construction, as well as to the complex ad innovative spatial solutions; the continuous experimentations in all these areas have been among the characteristic features of architectural and engineering research of the past century [1, 2]. Moreover, these constructions were built using techniques that at the time were still experimental and based on design criteria that did not consider seismic action. For these reasons, it is a priority to carry out a careful evaluation of the structural performances, both as regards the level of safety in static conditions and from the point of view of seismic behavior.

In particular, to understand the behavior and the vulnerabilities of heritage structures, the anamnesis process has to address aspects related to the identification of construction defects, deterioration, irregularities, the damage caused by previous events, and any factor that makes each of these structures unique and leads to a higher degree of complexity when interpreting the structural behavior [3, 4]. The experimental activities, including destructive and non-destructive tests, are part of those operations aimed at identifying the structural characteristics and determining the state of health of the structure. The purpose of this work is to analyze the state of conservation and the possible damage level of the pillar structures in Hall B by innovative non-destructive techniques. In particular AE analyses were performed on the vertical bearing structures supporting the undulated vault.

Detection of damage and faults in concrete structures and, more importantly, accurate identification and charac-

---

terization of internal flaws are vital aspects to ensure the safeguard of reinforced concrete structures and infrastructures. Over the last decades, various non-destructive testing (NDT) techniques have been developed and implemented to detect internal defects of structures in concrete [5, 6]. These NDT methods include ultrasonic damage detection, ground penetrating radar technologies, impact-echo, thermographic analysis, acoustic emission [7–12]. Among these different technologies, the impact-echo (IE) method is the

most widespread one employed for detecting cracks and delamination of concrete structures. The popularity of the IE method consist in its advantages of being actually non-invasive and non-destructive, suitable for single side detection, easy to use, having relatively greater detection depth, and less affected by differences in concrete materials and structures [5, 6]. The impact-echo technique, introduced by Carino and Sansalone [5, 6, 8], is based on analyzing the reflection signals of impact-induced stress waves propagating through the testing element/structure. In the present paper a particular application of the acoustic signal analysis based on IE technique is proposed. Through the IE approach, the evaluation of the AE signal velocity propagation is considered in order to evaluate a discrimination of the supporting elements of a monitored structure. As it is well known, propagation velocity of the acoustic signal (elastic wave) inside a medium is related to the elastic characteristics of the material itself. The P-wave propagation value in a steady state condition or in a particularly rapid evolutionary scenario represented an evident indicator of damaging state of a monitored structure under loading. In the context of the present work the relationship between the velocity of the acoustic signals and the elastic characteristics is evaluated in order to discriminate the stiffness level of the slant pillars constituting the structure under consideration. The procedure presented here has made it possible to develop a method of investigation capable of estimating, by means of AE monitoring, the state of conservation and the elastic properties of the monitored concrete structures.
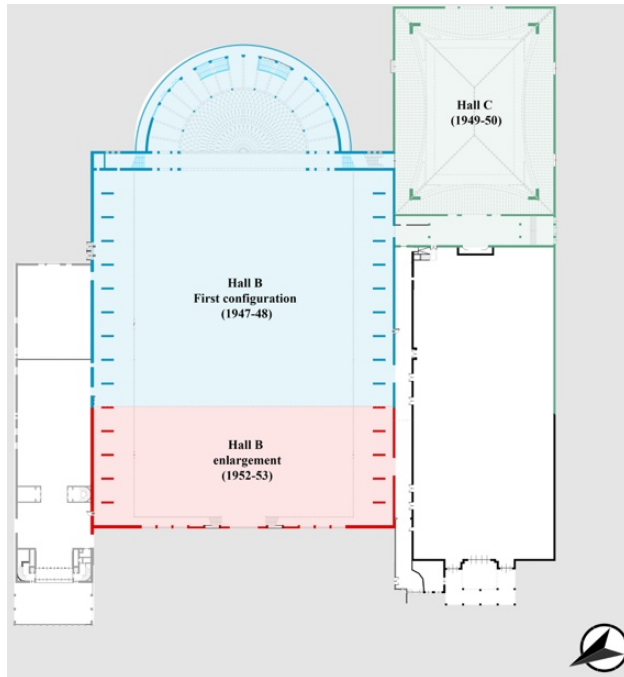
(a)

(b)

Figure 1: (a) Torino Esposizioni plan: the large hall with the semicircular apse is Hall B built in 1948 (in blue) and enlarged in 1953 (in red), and the smaller Hall C built in 1950 (in green). (b) An interior of Hall B after completion in 1948 (photo by Aldo Moisio)

2 The slanted pillars of hall B: the monitoring site

The Turin Exhibition Center was conceived immediately after the Second World War to host the annual Automobile Show, and was supported and promoted the Fiat motor company, located in Turin. The two main buildings of the complex, Halls B and C, represent an remarkable example of innovative use of the new advanced techniques in reinforced concrete construction, which combined the new prefabrication procedures and the re-invention of ferrocement by Nervi.

The ferrocement, whose use is here combined with extensive use of prefabrication, is adopted for its lightness, resistance and malleability to make structural elements resistant in shape, with extraordinary results from an aesthetic point of view. Nervi underlines these great expressive possibilities offered by the use of these techniques, affirm-

ing in the presentation of the structures of Hall C, which allow "*to release the reinforced concrete from the slavery of the formwork into lumber and open new and unlimited fields to the planning and static-architectural fantasy*" [13].

Hall B was inaugurated on 15 September 1948. The hall consists of a nave covered by an undulated vault, and of an apse with a ribbed semispherical dome. Hall B represents a milestone in the history of 20th century engineering and architecture. Moreover, in the literature on contemporary architecture, it is frequently referred to as Nervi's iconic masterpiece and as one of his most skillful examples of structural art. The Hall B in the Turin Exhibition center offered Nervi the first great occasion to apply to a large-scale project the principle of structural prefabrication, a method he experimented during the war years on small-scale building [14]. It is reported a plan of the whole complex in the Figure 1a, and an interior of the hall in the Figure 1b.

For the construction of the building, Nervi had to face a series of uncommon construction problems that were difficult to resolve using conventional building systems. He was allotted a limited amount of time for the construction and had to face the static problems due to the covering of the large hall requested by the client. Moreover, he had to face several financial cuts in the period characterized by material shortages. He was also constrained by the masterplan, prepared by the Fiat engineer Roberto Biscaretti di Ruffia, designed to rebuild a new complex on the remains of the Palazzo della Moda, bombed during the war. Nervi proposed to build a hall with two typologies of thin shells, undulated and ribbed, supported by reinforced concrete elements.

Apart from the analysis of the various elements of hall B, whose construction technology is better analyzed in [15], and seismic criticalities are instead highlighted in [16], the present paper focuses its attention on the inclined pillars. Nervi applied his personal design also on these elements: Biscaretti di Ruffia in his project envisage vertical elements, while Nervi modify them in inclined spurs, shaped in accordance with the force flow of the vault. As Greco underlined [17], the architectural and structural scheme of the inclined pillars had been experimented several times in the hangars of the thirties and is also reproduced in this project. The modularity of the system instantly characterizes the vaulted interior space of the hall, that expanded continuously in the lateral naves (Figure 1b). This modularity presents other advantages: in its first configuration, completed in 1948, Hall B measured 96 meters in width and 110 meters in length. Between 1952-1954, Hall B was enlarged by five spans in order to move the façade on the street and it reached the length of 155 meters. The enlargement was completed swiftly in a few months, demonstrating the

success of the Nervi's system. This characteristic makes the building a rare case of concrete application of the so-called "modular flexibility", and as Greco points out [17], this aspect has been neglected by critics. In order to reconstruct the construction stages of the building, Figure 1a, reports them in plan.

Nervi was given only ten months to complete the work, starting from August 1947. It is important to highlight that most part of the construction site took place during winter, and considering that the in-situ manufacture of the structural elements, Nervi had to worry about finding a solution for the curing of prefabricated concrete elements. If one considers also the difficulties of finding the materials in the years immediately after the war, the timeframe was incredibly tight.
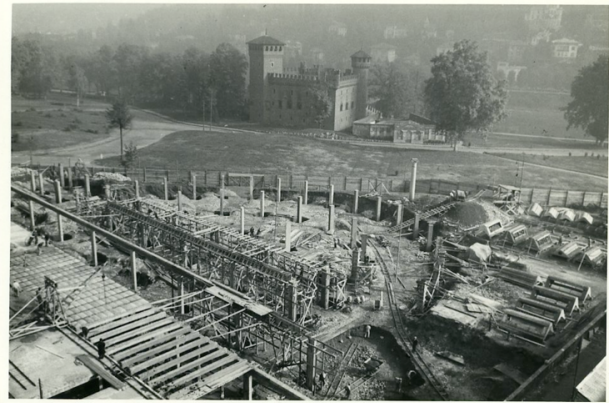
(a)
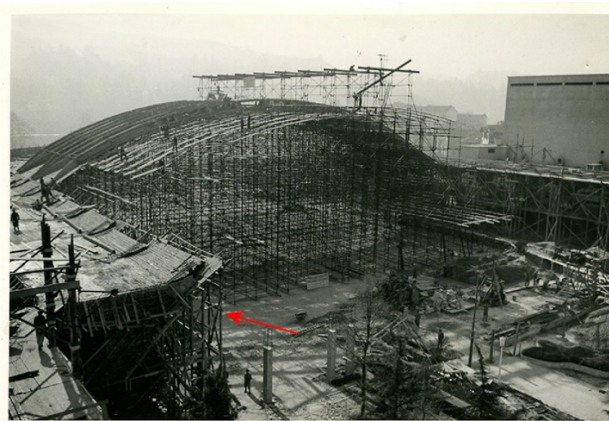
(b)

Figure 2: (a) A picture showing the initial stage of the construction site of hall B, which started from the apse. It is also possible to notice the prefabricated elements in ferrocement built simultaneously. (b) Advancement of the construction site, in which the red arrow indicates a pillar that has not been cast yet, while the ones closer to the apse are in a more advanced stage (photos by Riccardo Moncalvo)
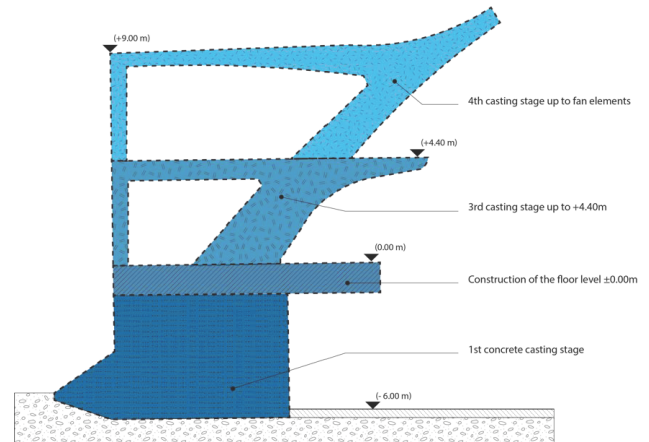
(a)

(a)
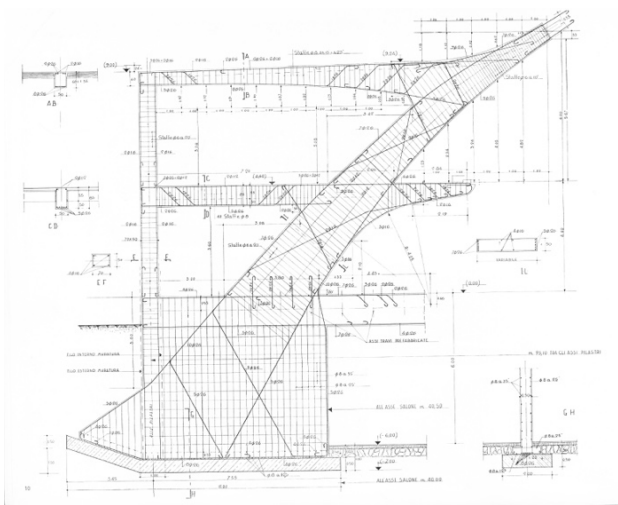
(b)

Figure 3: (a) Advancement of the construction site with the elevation of the first portion of the undulated vault (photos by Riccardo Moncalvo). (b) Detail of the reinforcing of the pillars and the connections with the slabs at the various levels and the fanned elements [18]

(b)

Figure 4: (a) Scheme of the various casting stages of pillars. (b) Detail of the interiors just after the completion of the hall (photo of Aldo Moisio)

In this overview, the proper planning of the construction site became crucial. The decomposition of the structure into a large number of elements equal to each other made it possible to start their execution from the first day and to continue in parallel with the preparation of the foundations and complementary structural elements. The time needed to build structures was optimized in this way.

The construction site started from so-called "apse", the round element with the ribbed half dome (Figure 2a). At the same time, workers started to build the prefabricated ferrocement elements of the undulated vault (Figure 2a).

Almost all the structural elements were built starting from this portion of the building. It is important to highlight that the inclined pillars were built in different stages, starting from the apse, and the vaulting followed accord-

ingly. In Figure 2b, a red arrow indicates a pillar that has not been cast, while the ones closer to the apse are in a more advanced stage. In fact, the scaffolding of the first section of the vault was built from the apse, and it was moved sequentially in the direction of the main façade. The scaffolding was moved only when the undulated elements

of a set of arches were set (Figure 3a). In the last stages, it was poured the concrete for the connections of the fanned elements and the pillars; subsequently, also elements of the undulated vault were completed with the casting of the ribs. Figure 3b reports the detail of the reinforcing of the pillars and the connections with the slabs at various levels and the fanned elements.

The fanned elements aren't just a formal expression of continuity between the vault and the pillars, but are actually a crucial structural element, that directs the reinforcement bars between the waves and the pillars. The bundles of reinforcement bars start in the pillars, separating in the fans, and then run along the hollows and ridges of the undulated elements of the vault [19]; in this way, Nervi connects together the prefabricated elements with the rest of the structure by pouring the concrete.

The supporting structures of the vault were instead built in four different stages, in which the concrete was poured sequentially in different months. Figure 4a shows a section of an inclined pillar reporting a scheme of the various casting stages, while Figure 4b shows a picture of the interiors just after the completion of the hall.

3 AE Monitoring and P-wave velocity estimation as a damage index for old concrete

In order to investigate the properties of the slant pillars, ND testing, based on AE measurements (ultrasounds), were performed on three different pillars that could present discrepancies in mechanical properties due to different causes: the casting procedures, that, as it was previously reported, was executed in different stages, and the enlargement of the hall happened a few years later. In addition, the purpose of the investigation is to evaluate if the adopted technique is able to discriminate between elements characterized by different mechanical characteristics (Young's modulus).

The tested pillars were selected as follows. The first investigated pillar (P4$_S$) belongs to the enlargement of the hall, which took place between 1952-53. The pillars named P8$_S$ and P13$_S$ are, instead, the part of the first configuration of the hall, built in 1948. However, according to the construction stages, P13$_S$ was built before P8$_S$. Given the fact that immediately after the war, the construction conditions were certainly not the best, it is possible to hypothesize that any difference in the timing of construction could have generated some flaws or at least some dissimilarities in the mechanical properties of the structural elements.

In order to carry out these tests, the ND procedures were performed by a technique coming from the impact-echo, allowing to obtain, as a parameter of estimation of the damage, the P-wave propagation velocity inside the monitored element. To this purpose, an array of 7 sensors has been placed on the surfaces of the pillars in correspondence to the last level (between quote +4.40 m and 9.00 m) represented in Figure 4a. In Figure 5a–5c, it is reported the arrangement of the sensors on the three slanted pillars and their arrangement on the monitored surface is reported. In Figure 5d the position of the sensors respect to the positions of the impact points of the hammering can be observed.
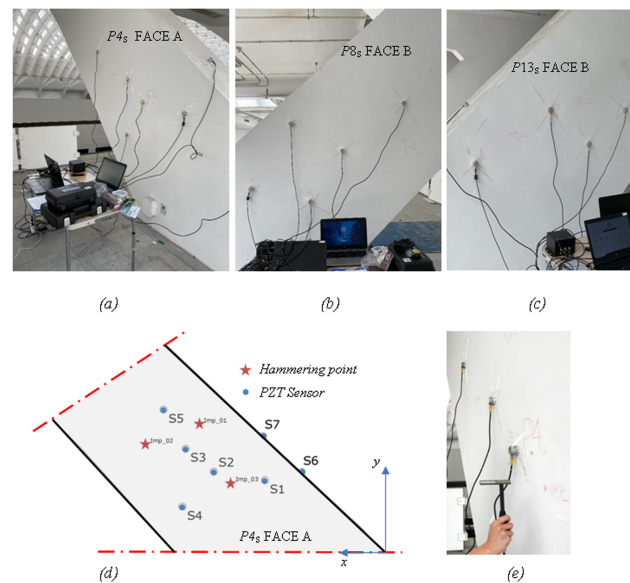

Figure 5: Application of the sensor array to the slant pillar (a) P4$_S$, (b) P8$_S$, (c) P13$_S$. (d) Detail of the sensor positions for P4$_S$. (e) Hammering performed on the surface of the pillar

In this case, the principle of impact echo was used considering the localization procedure, generally used in the traditional AE monitoring [20–23]. The signals were correlated to the hammering position source and, consequently, the velocity of the P-wave propagation was estimated. Generally, localization is one of the most used analyses in AE monitoring. The AE localization technique has been widely applied both in laboratory and in-situ tests and has been performed with different methods to improve the results accuracy [24–30]. In this paper, the triangulation technique was applied to signals recorded by at least five sensors falling into time sufficiently small intervals (50 μs). Thus, with this procedure, it is possible to define both the position of the source, which is known a priori, and the speed of longitudinal P-waves transmission in the medium. Having denoted with t_i the arrival time at a sensor S_i of an

AE event generated at point S and at time t_0 we have [23]:

$$|S - S_i| = \left[(x - x_i)^2 + (y - y_i)^2 + (z - z_i)^2\right]^{\frac{1}{2}} \quad (1)$$

the distance between S_i and source S, in Cartesian coordinates; and assuming the material to be homogenous, the path of the signal is given by $|S - S_i| = v_p(t_i - t_0)$. If the same event is observed from another sensor S_j at time t_j [23]:

$$\left|S - S_j\right| - |S - S_i| = v_p \left(t_j - t_i\right) \quad (2)$$

If the same event is observed from another sensor S_j at time t_j, it is possible to eliminate t_0 from the calculation. Assuming the arrival times of the signals and the positions of the two sensors to be known, the last is an equation with four unknowns x, y, z, and v_p. Hence, the problem of the localization of S is determined if it is possible to write a sufficient number of equations of that type (Eq. 2), *i.e.*, when the same AE event is identified by at least five sensors. If this does not occur, it is necessary to adopt simplifying assumptions to reduce the degrees of freedom of the problem, such as, for instance, imposing the speed of transmission of the signals (v_p) or having the AE source lie on a predetermined plane. For the analysis carried out in the present research, three-dimensional localizations with at least five sensors were performed. In the present case, in additions to the source coordinates, the unknown is specifically the P-wave propagation velocity (v_p). In any case, the localization was carried out in order to consider the results of velocity associated with the localized points found sufficiently close to the hammering positions. We consider the solution for v_p only in the cases where the localized sources were found inside a circle of radius 5 mm centered in the hammering targets. This choice increased the accuracy of the velocity estimation. Therefore, the test procedure was carried out, positioning the sensors on the external surface of the slanted pillars and considering three different impact points. For each positions 2 series of measurements, composed of 5 impacts of the hammer, were performed (see Figure 5d). From all these tests, writing a system of at least 4 equations of the type of Eq. (2), it was possible to find different velocities values for each of the three monitored pillars. As shown in the following, the evaluation of the AE wave propagation velocity by different localizations seems particularly useful. The velocity v_p, in fact, resulted directly correlated to the Lame' constants to the stiffness of the monitored medium (Young's modulus, E and shear elastic modulus G): $v_p^2 = (\lambda + 2\mu)/\rho$. Considering the constitutive equations of the solid, it is possible to write:

$$-v(1 + v)\frac{\sigma_x}{E} + \left(1 - v^2\right)\frac{\sigma_z}{E} = 0 \quad (3)$$

This equation is written considering the case of an elastic wave with propagating direction along the coordinate direction x. It is possible to define ϵ_x as a function solely of σ_x:

$$\epsilon_x = \frac{\sigma_x}{E} - \frac{v}{E}2\frac{v}{(1 - v)}\sigma_x = \frac{\sigma_x}{E}\left(1 - \frac{2v^2}{1 - v}\right) \quad (4)$$

After expressing the stress, its first and second derivative respect to x-direction they can be directly correlated to the propagation velocity of the elastic wave (vibration) assuming s an as the displacement along the direction x:

$$\sigma_x = \left(\frac{E(1 - v)}{(1 + v)(1 - 2v)}\right)\frac{\partial s_x}{\partial x} \quad (5)$$

$$\frac{\partial \sigma_x}{\partial x} = \left(\frac{E(1 - v)}{(1 + v)(1 - 2v)}\right)\frac{\partial^2 s_x}{\partial x^2} \quad (6)$$

at the same time, it is also possible to write that:

$$\frac{\partial \sigma_x}{\partial x} = \rho\frac{\partial^2 s_x}{\partial t^2} \quad (7)$$

where t is the time in which the propagation took place and ρ is the mass per unit volume. According to Eq. (6) and (7) we can write:

$$\frac{\partial^2 s_x}{\partial t^2} = \frac{\partial^2 s_x}{\partial x^2}\frac{1}{\rho}\frac{E(1 - v)}{(1 + v)(1 - 2v)} \quad (8)$$

The second term on the right side takes the dimensions of a squared velocity. The expression for v_p can be finally expressed as [29]:

$$v_p = \sqrt{\frac{E}{\rho}\frac{(1 - v)}{(1 + v)(1 - 2v)}} \quad (9)$$

and assuming the value of $v = 0.2$ for concrete we have the following relation to estimate the elastic modulus E:

$$E = 0.9\left(v_p^2\rho\right) \quad (10)$$

From Eq. (9), it is easy to observe how v_p is a function of the elastic modulus (E), the mass per unit volume ρ, and the Poisson's coefficient (v) of the material. In Figure 6, as an example, a graph of a typical AE acquisition, obtained during the hammering tests carried out on the slant pillar P4$_S$ of Hall B, is reported. As it can be seen, peaks correspond to the hammerings performed on one of the points of impact (Imp02). For each peak, there is a varying number from 5 to 7 of the AE signals detected in relation to the number of sensors that actually perceive the elastic propagation coming from the hammering. The frequency of the signals acquired by the sensors is reported with respect to the time employed for the test. The AE frequency evaluation appeared to be very important in the preliminary filtering
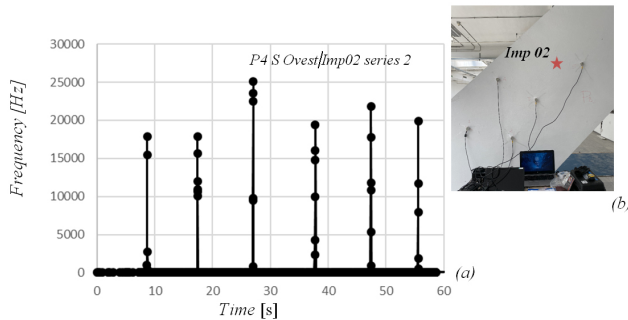
Figure 6: (a) Frequency vs time graph related to the acquisition of the acoustic signals due to the hammering in position imp02 (b)

of the signals. In the present study, a threshold of $1{\times}10^3$ Hz is considered. Signals acquired below this value were neglected because they definitely belonged to the background noise. The whole procedure is described in the flow-chart reported in Figure 7. The beginning of the acquisition is characterized by the generation of the artificial sources. In general, they may originate from a natural phenomenon (crack propagation or formation of micro-cracks) or from an artificial cause (impacts produced by a digital hammer). In the present case, the AE sources are generated by hammering on the external surface of the slanted pillars. During the perturbation created by the impact in the positions Imp01, 02 and 03 for each pillar, the AE signals were recorded. The acquisition is carried out for a duration of 60 s for each hammering sequence. After this, the first filtering is applied to AE signals (Figure 7). As previously mentioned, in the present experiments, only AE with a mean frequency greater than $1{\times}10^3$ Hz were considered. After this preliminary phase, the recognition of the data sets consistent with the localization procedure was performed. For the localizations, all pairs, triplets, quatrains, and so on that have the differences in the arrival times to sensors in the range $\Delta t_j - \Delta t_0 < 10 \times E^{-4}$ s were considered belonging to the same event (impact). In the analyzed case, the event generating the signals is the rhythmic hammering in the impact positions. Once these data sets are selected, a system of equations of the type of Eq. (2) can be written. The localization adopted is based on the triangulation technique and the improved AIC-method, as reported in Carpinteri *et al.* [23]. Once localized sources are obtained, and after verifying that the obtained results are localized close to the artificial source created ad hoc (maximum error accepted = 1%), the value of the p-wave propagation velocity (v_p) is extracted. Finally, through Eq. (10), it is possible to estimate the value of the elastic module (E) associated with the velocity v_p just calculated with the described method (Figure 7). In Figure 8a and 8b, the calculated v_p and the elastic
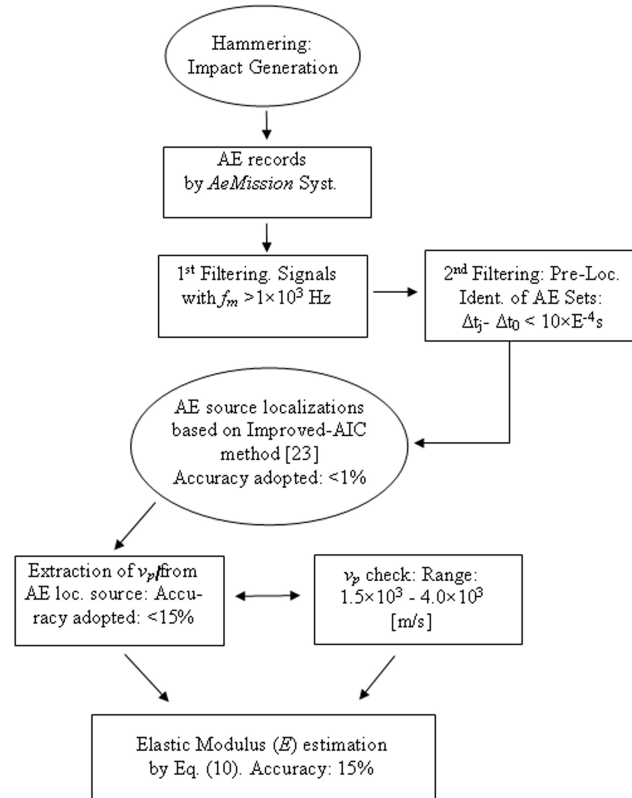

Figure 7: Flow-chart of the elastic modulus estimation by v_p measurements. Different steps are performed to reduce measurement errors. The localization procedure leading to the v_p values is based on the improved Akaike algorithm Criterion as reported in [23]

modulus estimation for each localization are reported together with the mean values for each of the three analyzed pillar: $P4_S$, $P8_S$, $P13_S$.

Figure 8 shows the results for velocity values obtained by 54 localizations on the three slanted pillar $P4_S$, $P8_S$, and $P13_S$. The values are reordered from the lower to the higher for each series. $P4_S$ resulted in being the element with the highest values in terms of v_p that corresponds to a higher level for the stiffness characteristics (*E*, *G*). The values reported for the $P4_S$ pillar start from very low values around $1.4{\times}10^3$ m/s up to values of about $3.7{\times}10^3$ m/s. The average velocity obtained from the localization of AE due to hammering is $2.5{\times}10^3$ m/s for $P4_S$. Similar considerations can be made for pillar $P8_S$. The velocity values for $P8_S$ range from values of around $1.8{\times}10^3$ m/s to $3.1{\times}10^3$ m/s. The average velocity obtained from the localizations of AE signals is about $2.3{\times}10^3$ m/s for the $P8_S$ pillar, slightly lower than that of pillar $P4_S$. Finally, as regards the values obtained for $P13_S$, different values are obtained. For the minimum set values, the lowest was about $0.9{\times}10^3$ m/s to a maximum value of about $2.9{\times}10^3$ m/s. The average velocity obtained in this case is equal to $1.9{\times}10^3$ m/s for pillar $P13_S$. It is evi-
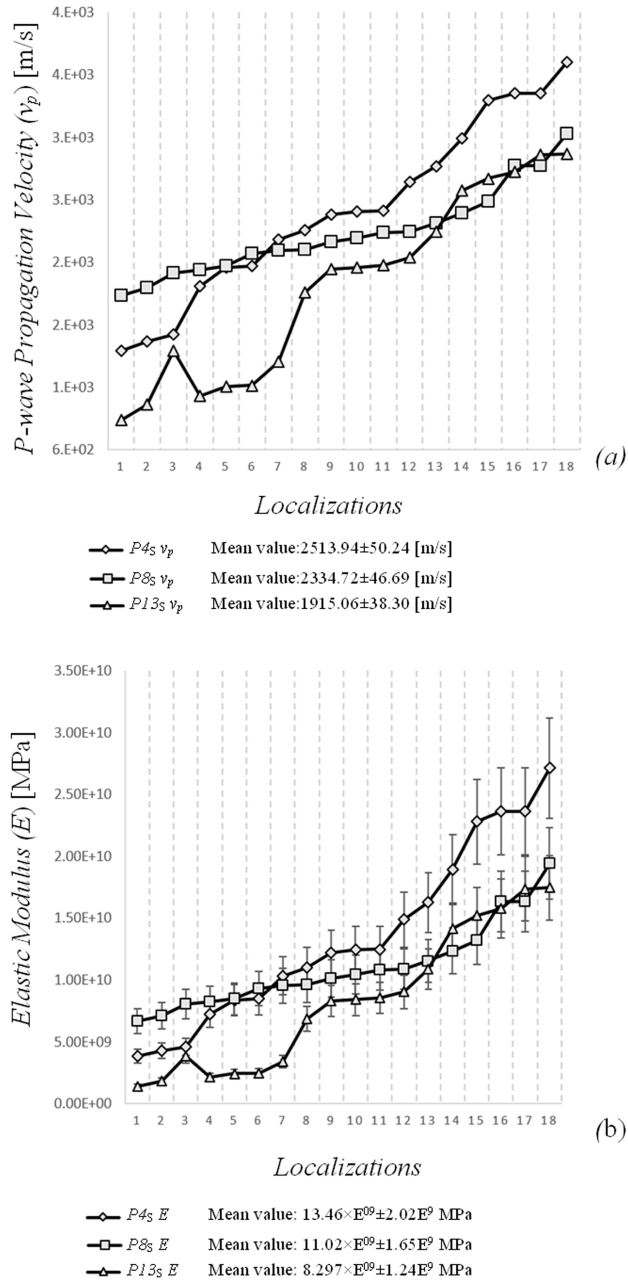
(a)

(b)

Figure 8: P-wave propagation velocities obtained by 54 localizations on the three slanted pillar P4S, P8S, P13S. The values were reordered considering increasing values for each series (a). $P4_S$ resulted in being the element with the highest speed values corresponding to a higher level of stiffness characteristics (E) (b)

dent that the averaged values of E, that will be calculated by Eq. (10) will be slightly under-estimated. This effect is certainly due to the presence of a layer of about 20 mm on the external surface of the three slant pillars formed by the plaster layer and the coating. This value can be considered with a reduction of the final value of about 1%. This reduction is estimated considering the proportion between the

medium distances between sources and sensors covered by AE signals in concrete and plaster. At the same time, the procedure to estimate the values of the elastic modulus carried out by the authors is certainly not devoid of measurement errors. As previously reported, in Figure 7, the flow-chart reports the different steps followed for the calculation of the values of v_p and to estimate the elastic modulus. In particular, in the present work, the localization procedure based on the data analysis of AE was used with an improved version of the Akaike Information Criterion was used for the estimation of v_p like one of the output coming from the triangulation technique [23]. This process allowed to calculate the unknowns of the equation system (source coordinates and v_p) with very high precision. For this reason, the values of v_p were considered with a maximum error measurement of $\Delta v_p = \pm 1\%$ (see Figure 7). For the calculation of the elastic modulus, in the absence of specific tests, the value for the density is 2.2×10^3 kg/m^3 and an assumed error $\Delta\rho = \pm 15\%$. Considering the theory of error propagation and the relation reported in Eq. (10), we can estimate the different values of E for the three slanted pillars. In Figure 8a, the v_p obtained from the localization procedures are reported together with the three mean values. In Figure 8b, the E values calculated by Eq. (10) are reported, also in this case, together with the three mean values, one for each of the analyzed pillars. The final error for each measurement is equal to $\pm 15\%$. The mean values of E returned us values equal to $13.46 \times E^{09} \pm 2.02 \times E^{09}$ MPa for $P4_S$, $11.02 \times E^{09} \pm 1.65 \times E^{09}$ MPa for $P8_S$, and $8.297 \times E^{09} \pm 1.24 \times E^{09}$ MPa for $P13_S$ (see Figure 8b). It is important to consider that, in the present paper, the main objective is represented by the difference between the stiffens of the monitored pillars. For this reason, it seems very useful to evaluate the ratios between the average elastic modulus found P8s and P13s pillars with respect to the value calculated for P4s:

$$\frac{E_{P8s}}{E_{P4s}} = 86.2 \pm 24.5\%; \tag{11a}$$

$$\frac{E_{P13s}}{E_{P4s}} = 58.0 \pm 18.5\%; \tag{11b}$$

Equations (11a) and (11b) have shown a reduction in the stiffness characteristics of the monitored concrete structures of about 13.8% and 42.0%, respectively, for $P8_S$ and $P13_S$ pillars with respect to $P4_S$. This evidence confirmed the hypotheses put forward in the context of the historical reconstruction of the building phases for Hall B. In particular, the first construction phases (P13s and P8s) are characterized by jets with a less performing conglomerate compared to the portion of the building concerning the last expansion.

4 Conclusions

In the present paper, the calculation of the velocity of the P-wave propagation of AE was used to evaluate the stiffness characteristics of slanted pillars constituting the vertical bearing structures designed by Pier Luigi Nervi in one of his most iconic building: the halls of Torino Esposizioni (Hall B). In order to investigate the properties of the inclined pillars, a triangulation procedure (source localization), based on AE measurements (ultrasounds) generated by artificial causes (hammering), were performed on three different pillars. These elements presented discrepancies due to different causes: the casting procedures, that, as it was previously reported, were executed in different stages, and the enlargement of the hall happened a few years later respect to the beginning of the construction. The purpose of the investigation was to evaluate if the adopted technique was able to discriminate between elements characterized by different mechanical characteristics (Young's modulus).

The tested pillars were selected as follows. The first investigated pillar ($P4_S$) belongs to the hall's enlargement, which took place between 1952-53. The pillars named $P8_S$ and $P13_S$ were, instead, located on the first configuration of the hall, built in 1948. However, according to the construction stages, $P13_S$ was built before $P8_S$. The AE measurements and, in particular, the P-wave velocity estimation confirmed the hypothesis. The average velocity obtained from the localizations of AE performed on $P4_S$ due to hammering was 2.5×10^3 m/s. The average velocity obtained from the localizations of AE in $P8_S$ was about 2.3×10^3 m/s for, slightly lower than that of pillar $P4_S$. Finally, concerning the values obtained for $P13_S$, the average velocity obtained in this case is equal to 1.9×10^3 m/s. The elastic modulus values calculated by Eq. (10), considering the average velocities, returned us values of about 13.5 MPa for $P4_S$, 11.0 MPa for $P8_S$, and 8 MPa for $P13_S$. It is evident that these average values of E are slightly under-estimated. According to Eqs. (11a) and (11b), the values showed a reduction in the stiffness characteristics of the monitored concrete structures to 86.2% and 58.0%, respectively for $P8_S$ and $P13_S$ pillars with respect to $P4_S$. This evidence confirmed the hypotheses put forward in the context of the historical reconstruction of the building phases for Hall B. In particular, the first construction phases ($P13_S$ and $P8_S$) were characterized by less performing stiffens of the concrete conglomerate with respect to the portion of the hall concerning the last expansion. On the basis of these findings, we can suppose that the expansion of the building was made with materials characterized by a higher performance. This implies that in view of a global analysis of the structure,

this possible and substantial difference must be considered. This information can be used to develop targeted interventions aimed at preserving the daring structures built in the 20$^{\text{th}}$ century. In particular, by highlighting differences and potential criticalities in the materials. NDT tests may represent a suitable method of characterization, especially for analyzing thin and fragile structural elements, such as ferrocement. A further step of the analysis will need to assess the characteristics of all the pillars, even at the different quotes. The procedure here reported made it possible to develop an innovative investigation method able to estimate, by means of AE, the state of conservation and the elastic properties and the damage level of the monitored concrete and reinforced concrete structures.

Author contributions: All authors have accepted responsibility for the entire content of this manuscript and approved its submission.

Conflict of interest: The authors state no conflict of interest.

References

[1]   Croft C, Macdonald S, Ostergren G. Concrete: Case Studies in Conservation Practice. Getty Publications; 2019.
[2]   ICOMOS International Committee on Twentieth Century Heritage (ISC20C), Approaches for The Conservation of Twentieth-Century Cultural Heritage, 2017.
[3]   Ceravolo R, De Lucia G, Lenticchia E, Miraglia G. Seismic Structural Monitoring of Cultural Heritage Structures. Springer; 2019:51–85.
[4]   ICOMOS, Principles for the analysis, conservation and structural restoration of architectural heritage, 2003.
[5]   Sansalone M, Streett W. Impact-Echo: Nondestructive Evaluation of Concrete and Masonry. Ithaca, NY, USA: Bullbrier Press; 1997.
[6]   Sansalone M. Impact-Echo: the complete story. ACI Struct J. 1997;(94):777–86.

[7] Valenzuela M, Sansalone M, Streett W, Krumhansl C. Use of sound for the interpretation of impact-echo signals. In: *Proc 4th Int Conf Audit Displ (ICAD1997)*, Palo Alto, CA, USA, 2–5 November, 1997.

[8] Carino N, Sansalone M, Hsu N. A point sourcepoint receiver, pulse-echo technique for flaw detection in concrete. ACI J. 1986;(83):199–208.

[9] Lacidogna G, Manuello A, Carpinteri A, Niccolini G, Agosto A, Durin G. Acoustic and electromagnetic emissions in rocks under compression. Experimental Mechanics on Emerging Energy Systems and Materials. 2011;5:57–64.

[10] Niccolini G, Bosia F, Carpinteri A, Lacidogna G, Manuello A, Pugno N. Self-similarity of waiting times in fracture systems. Phys Rev E Stat Nonlin Soft Matter Phys. 2009 Aug;80(2 Pt 2):026101.

[11] Niccolini G, Durin G, Carpinteri A, Lacidogna G, Manuello A. Crackling noise and universality in fracture systems. J Stat Mech. 2009;01(01 no. P01023):P01023.

[12] Lacidogna G, Manuello A, Niccolini G, Carpinteri A. Acoustic emission monitoring of Italian historical buildings and the case study of the Athena temple in Syracuse. Archit Sci Rev. 2015;58(4):290–9.

[13] Nervi PL, La struttura portante del nuovo Salone del Palazzo di Torino Esposizioni, *Rassegna tecnica della Società degli ingegneri e architetti in Torino*, (in Italy); 1950.

[14] Chiorino C. Problems and strategies for documentation and conservation of Pier Luigi Nervi's heritage, The case study of Turin. Journal of the IASS. 2013;54(176 & 177):221–32.

[15] Greco C. The "ferro-cemento" of Pier Luigi Nervi, the new material and the first experimental Building, In: *Proc Int Symp IASS*, Padova, 1995.

[16] Lenticchia E, Ceravolo R, Antonaci P. Sensor Placement Strategies for the Seismic Monitoring of Complex Vaulted Structures of the Modern Architectural Heritage. Shock Vibration. 2018:3739690.

[17] Greco C., Nervi PL. Dai primi brevetti al Palazzo delle Esposizioni di Torino 1917-1948, Lucerna: Lucerne Quart Edizioni, 2008.

[18] Nervi P. Aesthetics and Technology in Building, The Charles Eliot Norton Lectures ed., Harvard University Press, 1965.

[19] Gargiani R, Bologna A. The rhetoric of Pier Luigi Nervi. Concrete and ferrocement forms. Lausanne: EPFL press; 2016.

[20] Carpinteri A, Lacidogna G, Niccolini G, Puzzi S. Critical defect size distributions in concrete structures detected by the acoustic emission technique. Meccanica. 2007;43(3):349–63.

[21] Carpinteri A, Lacidogna G, Niccolini G. Acoustic emission monitoring of medieval towers considered as sensitive earthquake receptors. Nat Hazards Earth Syst Sci. 2007;7(2):251–61.

[22] Lacidogna G, Manuello A, Niccolini G, Carpinteri A. Acoustic emission monitoring of Italian historical buildings and the case study of the Athena temple in Syracuse. Archit Sci Rev. 2012;58(4):1–10.

[23] Carpinteri A, Xu J, Lacidogna G, Manuello A. Reliable onset time determination and source location of acoustic emissions in concrete structures. Cement Concr Compos. 2012;34(4):529–37.

[24] Niccolini G, Durin G, Carpinteri A, Lacidogna A, Manuello A. Crackling noise and universality in fracture systems, J Stat Mech Theory Exp. 2009:P01023.

[25] Niccolini G, Bosia F, Carpinteri A, Lacidogna G, Manuello A, Pugno N, Self-similarity of waiting times in fracture systems. Phys. Rev. E, 2009;80:26101/1–26101/6.

[26] Manuello A, Masera D, Carpinteri A. Acoustic Emission Monitoring of the Turin Cathe-dral Bell Tower: Foreshock and Aftershock Discrimination. Appl Sci (Basel). 2020;10(11):3931.

[27] Carpinteri A, Lacidogna G, Manuello A. Damage Mechanisms Interpreted by Acoustic Emission Signal Analysis. Key Eng Mater. 2007;347:577–82.

[28] Shiotani T, Yuyama S, Li Z, Ohtsu M. Application of AE improved b-value to quantitative evaluation of fracture process in concrete materials. J Acoust Emiss. 2001;19:118–32.

[29] Shiotani T, Fujii K, Aoki T, Amou K. Evaluation of progressive failure using AE sources and improved b-value on slope model test. Prog. Acoust. Emiss. 1994;7:529–34.

[30] Ohtsu M, Kaminaga Y, Munwam M. Experimental and numerical crack analysis of mixed-mode failure in concrete by acoustic emission and boundary element method. Constr Build Mater. 1999;13(1-2):57–64.